

# Discrete scale invariance in fractals and multifractal measures

Wei-Xing Zhou<sup>1,2,\*</sup> and Didier Sornette<sup>2,3,4,†</sup>

<sup>1</sup>*State Key Laboratory of Chemical Reaction Engineering,*

*East China University of Science and Technology, Shanghai 200237, China*

<sup>2</sup>*Institute of Geophysics and Planetary Physics, University of California, Los Angeles, CA 90095*

<sup>3</sup>*Department of Earth and Space Sciences, University of California, Los Angeles, CA 90095*

<sup>4</sup>*Laboratoire de Physique de la Matière Condensée,*

*CNRS UMR 6622 and Université de Nice-Sophia Antipolis, 06108 Nice Cedex 2, France*

(Dated: May 23, 2019)

The theory of fractals and multifractals and their scaling laws provide a quantification of the complexity of a variety of scale invariant complex systems. We derive in this work the equations governing the concepts of discrete scale invariance (DSI) and the associated complex exponents in fractals, in multifractal measures and in joint multifractal measures. The set of complex exponents lie symmetrically with respect to the real axis in a vertical strip in the complex plane. In the lattice case, the set of complex exponents lie on finitely many vertical lines periodically and the DSI leads to the log-periodic corrections to scaling implying a preferred scaling ratio that is proved to be independent of the order of the moments. We perform detailed numerical analysis on lattice multifractals and explain the origin of three different scaling regions found in the moments. A novel numerical approach is proposed to extract the log-frequencies. In the non-lattice case, there are no visible log-periodicity, i.e., no preferred scaling ratio since the set of complex exponents are spread irregularly within the complex plane. A non-lattice fractal or multifractal can be approximated by a sequence of lattice fractals or multifractals so that the sets of complex exponents of the lattice sequence converge to the set of complex exponents of the non-lattice one. An algorithm for the construction of the lattice sequence is proposed explicitly.

PACS numbers: 05.45.Df, 02.50.Ey, 61.43.Hv, 47.53.+n

## I. INTRODUCTION

The word fractal was coined by Mandelbrot to describe sets, which consist of parts similar to the whole and which can be described by a fractal dimension [1], which is in the most case a fractional number. Meanwhile, multifractals were introduced to characterize the statistics of the strength of singularity of self-similar measures carried on geometric support [2, 3, 4, 5, 6]. Fractals and multifractals have been extensively introduced in the analysis of a wide class of phenomena in physics, geophysics, chemical engineering, turbulence, growth phenomena, and so on. At the same time, new ingredients were added in the theory of multifractals. Based on the discovery of anomalies in DLA, the phenomenon of phase transition in the multifractal spectrum was found and studied [7, 8, 9]. This led to the mathematical framework of the so-called left-sided multifractals [10, 11, 12, 13]. The vector-valued multifractals were introduced to formulate nonconservative measures such as the velocity field of turbulence [14]. Continuous multifractals [15, 16, 17] were adopted to quantify the droplets breakup in turbulent jet flows [18], which generalize the multipliers from discrete to continuous.

Another important concept is the negative dimension or latent dimension [19, 20, 21]. The physical implica-

tion of negative dimensions was discussed firstly in [22]. In practice, most of the physical processes are random, which leads to the phenomenon of sample-to-sample fluctuations of the multifractal function  $f(\alpha)$  by an amount greater than what the error bars on any single sample would indicate. In general, negative dimensions arise in such random multifractals [23, 24]. The randomness of multifractals at least arises in two situations where negative dimensions may emerge [23, 24]. First, one may obtain a multifractal constructed by a multiplicative cascade that is inherently probabilistic and the negative dimensions, if they exist, describe the rarely occurring events. Second, one may have to investigate the experiment from a probabilistic viewpoint. For instance, one-dimensional cuts of a deterministic measure carried out using a deterministic Sierpinski sponge will inevitably introduce randomness and may be regarded as random samples of a population. It is worth remarking that randomness in multinomial measures does not imply the existence of negative dimensions [25]. Actually, the multifractal slice theorem [26, 27] presents a mathematical interpretation of negative dimensions and is the basis of experimental measurement of lower dimensional cuts when the ensemble measurement is difficult to be carried out, which makes rigorous some aspects of Mandelbrot's intuition that negative dimensions may be explained geometrically by considering cuts of higher dimensional multifractals.

In the context of fractals and multifractals, scale invariance is the most important concept and characterizes

\*Electronic address: wxzhou@moho.ess.ucla.edu

†Electronic address: sornette@moho.ess.ucla.edu

fractals or multifractal measures in the form

$$\mathcal{O}(r) = \ell \mathcal{O}(\lambda r), \quad (1)$$

where  $\mathcal{O}$  is the observable and  $\lambda$  is the magnification factor or scaling ratio. In the common sense,  $\lambda$  is a continuous parameter resulting in the so-called continuous scale invariance (CSI). However, CSI is not always true when investigating fractals and multifractals. The general solution to Eq. (1) is

$$\mathcal{O}(r) = r^{-D} \psi(r), \quad (2)$$

where  $D$  is the fractal dimension and  $\psi(\lambda r) = \psi(r)$  is a log-periodic function with period  $\ln \lambda$  [28] (the term “log-periodic” means that the function  $\psi$  is periodic in the variable  $\ln r$  with period  $\ln \lambda$ ). Actually, the recently proposed discrete scale invariance (DSI) and its associated complex dimensions are an elaboration of the concept of scale invariance in which that system is scale invariant only under powers of specific values of the magnification factor (see [29] for a review). DSI with the signature of log-periodic oscillations decorating power law have been reported in several practical applications, such as in material rupture [30, 31, 32], earthquake precursors [33, 34], DLA [30, 35], turbulence [36, 37, 38], and economics [39]. In addition, there are also reports in the theoretical aspects of fractals [28, 40] and multifractals [41]. Notice the evolution of the concept of dimension from integer to fractional to negative and finally to complex, each time with precise physical meaning.

However, Eq. (1) is only a special (lattice) case of DSI [42]. In this work, we shall study the general framework of DSI in strictly self-similar fractals and multifractal measures. In Sec. II, we derive the basic DSI equations for fractals, for multifractal measures and for joint multifractal measures based on the self-similarity in moments. The structure of the complex exponents will also be discussed in both lattice and non-lattice cases. We then perform extensive numerical simulations on lattice multifractal measures to investigate different scaling regimes stemming from finite size effects in Sec. III. We propose a novel approach for the extraction of log-periodicity in the lattice case in Sec. IV. We conclude in Sec. V.

## II. GENERAL FRAMEWORK OF DISCRETE SCALE INVARIANCE IN FRACTALS AND MULTIFRACTALS

### A. Revisiting DSI in fractals

Smith et al [28] studied three Cantor sets with the initiators being 101 (the classic Cantor set), 101001001, and 101010001. They followed the G-P approach [43] and investigated the periodic oscillations in the log-log plot of the correlation integral  $C(\ell)$  with respect to scale  $\ell$ . In this section, we revisited DSI in the classic Cantor set using an alternative approach.

In order to generalize to other self-similar fractal sets, consider a fractal set  $\mathcal{F}$ , which is the union of  $n$  disjoint parts  $\mathcal{F}_i$ , namely  $\mathcal{F} = \cup_{i=1}^n \mathcal{F}_i$  with  $\mathcal{F}_i \cap \mathcal{F}_j = \emptyset$  for  $i \neq j$ . Let  $N(\mathcal{F}; r)$  be the number of boxes covering  $\mathcal{F}$  with scale  $r$ . We assume that the magnification of  $\mathcal{F}_i$  by a factor  $\lambda_i$  results in  $\mathcal{F}$ . This leads to

$$N(\mathcal{F}_i; r) = N(\mathcal{F}; \lambda_i r). \quad (3)$$

Note that the reciprocal of the amplification factor,  $1/\lambda_i$ , is called the scale multiplier. Since

$$N(\mathcal{F}; r) = \sum_{i=1}^n N(\mathcal{F}_i; r), \quad (4)$$

we obtain

$$N(\mathcal{F}; r) = \sum_{i=1}^n N(\mathcal{F}; \lambda_i r), \quad (5)$$

Equation (5) has a solution if and only if there exist integers  $k_i$  and  $\lambda$  satisfying

$$\lambda_i = \lambda^{k_i}, \quad (6)$$

which is the generalization of the Fibonacci rule of the number of maxima of the WTMM skeleton at a given scale in diffusion-limited aggregation [35] and corresponds to the called the lattice case [42]. The solution can be expressed as

$$N(\mathcal{F}; r) = r^{-D} \psi(r). \quad (7)$$

where  $\psi(r) = \psi(\lambda r)$  and  $D$  is the fractal dimension determined by the real solution of equation

$$\sum_{i=1}^n \lambda_i^{-D} = 1. \quad (8)$$

We see that  $N(\mathcal{F}; r)$  exhibits log-periodic oscillations with respect to  $r$ . Since  $N(\mathcal{F}; 1) = 1$ , it follows that  $\psi(\lambda^{-\ell}) = 1$ , where  $\ell \in \mathbb{Z}^-$ . For  $k_i = 1$ , we recover Eq. (1).

### B. DSI in multinomial measures

#### 1. General equation of DSI in multinomial measure

We construct a self-similar multinomial measure  $\mu$  supported by a set  $\mathcal{F}$  by a repeated  $n$ -based multiplicative cascade, where  $\mathcal{F}$  can be an Euclidean set or a fractal set of dimension  $\dim \mathcal{F}$ . In the first step, the support  $\mathcal{F}$  carrying some measure  $\mu$  is partitioned into  $n$  small pieces  $\mathcal{F}_i$  with  $i = 1, \dots, n$  based on some given set of scale amplification factors

$$\lambda_i = \|\mathcal{F}\| / \|\mathcal{F}_i\|, \quad (9)$$

where the measure is redistributed on  $\mathcal{F}_i$  according to a set of given multipliers:

$$m_i = \mu(\mathcal{F}_i; r/\lambda_i)/\mu(\mathcal{F}; r). \quad (10)$$

In the next step, each piece  $\mathcal{F}_i$  is further partitioned into  $n$  smaller pieces according to the same amplification factors  $\lambda_i$  and its carrying measure is redistributed again with the same multipliers  $m_i$ . This procedure continues *ad* infinity. So far, we have constructed a deterministic self-similar multinomial measure. Define a  $q$ -order moment function

$$\Gamma(\mathcal{F}; r, q) = \sum_r \mu^q(\mathcal{F}; r), \quad (11)$$

where  $\mu(\mathcal{F}; r)$  is the measure in an arbitrary box of scale  $r$  and  $\sum_r$  represents the sum over all boxes which result from partitioning  $\mathcal{F}$  with scale  $r$ . When we use boxes of size  $r$  to cover  $\mathcal{F}$ , the minimum number of disjoint boxes is  $\lceil \|\mathcal{F}\|/r \rceil$ . One finds easily that there might exist a box covering a part of  $\mathcal{F}$  whose size is less than  $r$ . In this case, we can arrange the  $\lceil \|\mathcal{F}\|/r \rceil$  boxes in a row (like a string) and cover  $\mathcal{F}$  in infinitely different ways by translating the boxes string along  $\mathcal{F}$ , thus introducing a random “phase.” This phase is one source of noise in the box-counting method. When  $r$  is small enough, the noise is reduced greatly so that the moments corresponding to different phases are approximately identical. In other words, the moment function is not affected by the partition procedure and we have

$$\Gamma(\mathcal{F}; r, q) = \sum_{i=1}^n \Gamma(\mathcal{F}_i; r, q). \quad (12)$$

Substitution of Eq. (10) in Eq. (11) leads to

$$\Gamma(\mathcal{F}_i; r, q) = m_i^q \Gamma(\mathcal{F}; \lambda_i r, q), \quad (13)$$

which shows the self-similarity of the moments. Combination of Eqs. (12) and (13) gives

$$\Gamma(\mathcal{F}; r, q) = \sum_{i=1}^n \Gamma(\mathcal{F}; \lambda_i r, q) m_i^q. \quad (14)$$

This is the basic DSI equation of the deterministic self-similar multinomial measures. For statistically self-similar measures [44], Eq. (14) can be revised as

$$\Gamma(\mathcal{F}; r, q) = \sum_{j=1}^k \sum_{i=1}^n \Gamma(\mathcal{F}; \lambda_{i,j} r, q) m_{i,j}^q p_j, \quad (15)$$

where  $p_j$  is the probability of choosing the  $j$ -th rule out of the  $k$  rules and  $\lambda_{i,j}$  and  $m_{i,j}$  are accordingly the scaling ratios and measure multipliers [25].

## 2. Solution of lattice multifractals

In the case of  $q = 0$ , the moment function equals to the number of partitioned boxes  $\Gamma(\mathcal{F}; r, 0) = N(\mathcal{F}; r)$ , which recovers Eq. (5).

If  $\lambda_1 = \dots = \lambda_n \equiv \lambda$ , it follows from Eq. (14) that

$$\Gamma(\mathcal{F}; r, q) = \Gamma(\mathcal{F}; \lambda r, q) \sum_{i=1}^n m_i^q. \quad (16)$$

In the formalism of multifractals, one expects that

$$\Gamma(\mathcal{F}; r, q) \propto r^{\tau(q)}, \quad (17)$$

where the scaling exponent of the moment is in the form

$$\tau(q) = -\ln \sum_{i=1}^n m_i^q / \ln \lambda. \quad (18)$$

In general, the solution to Eq. (16) is

$$\Gamma(\mathcal{F}; r, q) = r^{\tau(q)} \psi(r), \quad (19)$$

where  $\psi(r) = \psi(\lambda r)$  and  $\tau(q)$  is defined in Eq. (18). Since  $\Gamma(\mathcal{F}; 1, q) = 1$ , we have  $\psi(\lambda^{-\ell}) = 1$ , where  $\ell \in \mathbb{Z}^-$ .

Now, consider the case of lattice multifractals with the scale multipliers  $\lambda_i$  satisfying condition (6). It follows from (14) that

$$\Gamma(\mathcal{F}; r, q) = \sum_{i=1}^n \Gamma(\mathcal{F}; \lambda_i^k r, q) m_i^q. \quad (20)$$

It is easy to verify that Eq. (19) is also the general solution to Eq. (20), where  $\tau(q)$  is the unique real solution of

$$\sum_{i=1}^n \lambda_i^{k_i \tau(q)} m_i^q = 1, \quad (21)$$

We emphasize that  $\psi$  is  $q$  related but independent of  $\lambda$ . Also, the general solution of Eq. (15) has the same form of (19) with different “ $\tau(q)$ -generation function” in the lattice case.

## 3. Oscillations of other characteristic functions of multifractals

It is natural to investigate oscillations of other functions characterizing multifractals, namely, generalized dimensions  $D_q(r)$ , strengths of singularity  $\alpha(r, q)$ , and the multifractal function  $f(r, \alpha)$  or  $\tilde{f}(r, q)$  [3, 4, 5, 6], when one investigates scaling laws in some experimental data as well as simulated data. Our analysis is performed in terms of the variable  $r$  since all these functions vary with  $r$ . As usual, we define the exponent function of the moments as

$$\tau(r, q) = d \ln \Gamma(r, q) / d \ln r. \quad (22)$$

In equation (22), we remove the symbol of the support  $\mathcal{F}$  and use  $\tau(r, q)$  instead of  $\tau(q)$  as is used in [3, 4]. Simple algebraic calculations on equation (19) leads to

$$\tau(r, q) = \tau(q) + \Psi(r, q), \quad (23)$$

where

$$\Psi(r, q) = \frac{r\psi'(r)}{\psi(r)}, \quad (24)$$

Similarly, we have

$$D_q(r) \triangleq \lim_{q' \rightarrow q} \frac{\tau(r, q)}{q' - 1} = D_q + \lim_{q' \rightarrow q} \frac{\Psi(r, q')}{q' - 1}, \quad (25)$$

$$\alpha(r, q) \triangleq \frac{\partial \tau(r, q)}{\partial q} = \alpha(q) + \frac{\partial \Psi(r, q)}{\partial q}, \quad (26)$$

and

$$\tilde{f}(r, q) \triangleq q\alpha(r, q) - \tau(r, q) \quad (27)$$

$$= \tilde{f}(q) + q \frac{\partial \Psi(r, q)}{\partial q} - \Psi(r, q). \quad (28)$$

Hence, the four characteristic functions of multifractals,  $D_q(r, q)$ ,  $\tau(r, q)$ ,  $\alpha(r, q)$ , and  $\tilde{f}(r, q)$ , are all log-periodic in  $r$  with the same period  $\ln \lambda$ , which is independent of the order  $q$ . This result was verified in an experimental situation by extracting the log-periodicity of the moments of the energy dissipation in three-dimensional fully developed turbulence [38]. We shall return to this issue in Sec. IID.

### C. DSI in joint multifractal measures

In complex systems, there may be more than one self-similar measure embedded in the same sample space or phase space. For instance, in heated turbulent flow, both the energy dissipation rate  $\epsilon$  and scalars, say concentration  $C$  or temperature  $T$ , are known to be multifractal. Thus, it is interesting to consider the joint multifractal measures. Suppose that  $\mu_j$  with  $j = 1, \dots, l$  are  $l$  self-similar measures embedded in  $\mathcal{F}$ . The joint moments of order  $q = \sum_{j=1}^l q_j$  of the  $l$  measures are given by

$$J(\mathcal{F}; r, q) = \sum_r \prod_{j=1}^l \mu_j^{q_j}(\mathcal{F}; r). \quad (29)$$

The measure multipliers of  $\mu_j$  are defined by

$$m_{i,j} = \mu_j(\mathcal{F}; r/\lambda_i) / \mu_j(\mathcal{F}; r). \quad (30)$$

Combining (29) and (30), we have

$$J(\mathcal{F}_i; r, q) = J(\mathcal{F}; \lambda_i r, q) \prod_{j=1}^l m_{i,j}^{q_j}. \quad (31)$$

It follows from the additive rule of the joint moment

$$J(\mathcal{F}; r, q) = \sum_{i=1}^n J(\mathcal{F}_i; r, q) \quad (32)$$

that the DSI equation is

$$J(\mathcal{F}; r, q) = \sum_{i=1}^n J(\mathcal{F}; \lambda_i r, q) \prod_{j=1}^l m_{i,j}^{q_j}, \quad (33)$$

for deterministic measures where  $\lambda_{i,j}$  and  $m_{i,j}$  are the  $i$ -th multipliers of  $\mu_j$  or

$$J(\mathcal{F}; r, q) = \sum_{k=1}^{n'} \sum_{i=1}^n J(\mathcal{F}; \lambda_{i,k} r, q) \prod_{j=1}^l m_{i,j,k}^{q_j} p_k, \quad (34)$$

for statistically self-similar measures where  $\lambda_{i,k}$  and  $m_{i,j,k}$  are  $i$ -th multipliers of  $\mu_j$  for  $k$ -th rule with probability  $p_k$ .

Similarly, if  $\mu_j$  satisfy the lattice condition so that  $\lambda_{i,k} = \lambda^{k_{i,k}}$ , the general solution of Eq. (34) is

$$J(\mathcal{F}; r, q) = r^{\tau(q_1, \dots, q_l)} \psi(r), \quad (35)$$

where  $\psi(r) = \psi(\lambda r)$  and  $\tau(q_1, \dots, q_l)$  is the unique real solution of the following equation:

$$\sum_{k=1}^{n'} \sum_{i=1}^n \lambda_{i,k}^{\tau(q_1, \dots, q_l)} \prod_{j=1}^l m_{i,j,k}^{q_j} p_k = 1. \quad (36)$$

Again, since  $J(\mathcal{F}; 1, q) = 1$ , we have  $\psi(\lambda^{-\ell}) = 1$ , where  $\ell \in \overline{\mathbb{Z}^-}$ . The deterministic case Eq. (33) can be viewed as a special case of Eq. (34) with  $n' = 1$ .

It is clear that the DSI equations of multifractal measures in Sec. IIB are special cases of those of the joint multifractal measures with  $l = 1$ . Moreover, their DSI equations are the same in essence despite the possible difference in the coefficients. We expect to confirm the relevance of these formulas in real systems with hierarchical structures, especially in turbulence.

### D. Complex exponents

The previous sections emphasized the log-periodic structure of lattice fractals and multifractals. However, there is no log-periodicity for the non-lattice case. Instead, we can adopt the more general concept of complex exponents as was done in the former literature [29, 42]. Indeed, log-periodicity is only a special case of complex exponents in the lattice case, while complex exponents exist for both lattice and non-lattice fractals and multifractals. The complex dimensions of fractal strings were extensively studied from a mathematical point [42]. We note that a fractal string is not identical to the original fractal but to its complement. Hence, we propose a different approach, even for the fractals discussed in the previous sections. In this section, we study the structure of complex exponents in the complex plane and then provide an explicit algorithm for the construction of a sequence of lattice multifractals approximating a non-lattice multifractal whose set of complex exponents is the limit set of the sets of complex exponents of the lattice sequence.

### 1. The structure of complex exponents

In the previous sections, we assume that  $\tau(q)$  is real, thus the prefactor of the scaling relation  $\Gamma(r, q) \propto r^{\tau(q)}$  is a function of  $r$  in the lattice case, as expressed in Eq. (19). Expanding of  $\psi$  in the Fourier space yields complex exponents [29]. Therefore, we can assume that  $\tau(q)$  is complex so that the prefactor of the scaling relation is independent of  $r$ . In this sense, we have

$$\sum_{i=1}^n m_i^q \lambda_i^{\tau(q)} = 1. \quad (37)$$

A more general formulae was presented in Eq. (36). The solutions of Eq. (37) in the complex plane are denoted as

$$\tau(q) = \tau_R(q) + i\tau_I(q), \quad (38)$$

where  $i = \sqrt{-1}$  is the imaginary unit. We shall study this Eq. (37) in the sequel. The results are the same for the stochastic case.

For convenience, let  $h(\tau) = \sum_{i=1}^n m_i^q \lambda_i^\tau - 1$ . Since  $h(-\infty) = \infty$  and  $h(\infty) = -1$ , and because  $h(\tau)$  is continuous, real solutions to (37) exist. Moreover,  $h(\tau)$  is differentiable and we have  $dh(\tau)/d\tau < 0$ . Thus Eq. (37) has a unique real solution, denoted as  $\tau^R(q)$  hereafter. The geometric properties of  $\tau^R(q)$  are well-known [6]. As for the complex solutions, it is easy to show from the real value of  $h(\tau)$  that, if  $\tau(q)$  is a solution to (37), then  $\bar{\tau}(q) = \tau_R(q) - i\tau_I(q)$  is also a solution. Therefore the set of complex exponents are symmetric with respect to the real axis (they come in pairs of complex conjugates).

Let  $\tau(q)$  be a solution of Eq. (37). Then  $\tau_R(q) \geq \tau^R(q)$ . Otherwise, by assuming that  $\tau_R(q) < \tau^R(q)$ , we have  $|\sum_{i=1}^n m_i^q \lambda_i^{\tau(q)}| \leq \sum_{i=1}^n m_i^q \lambda_i^{\tau_R(q)} < \sum_{i=1}^n m_i^q \lambda_i^{\tau^R(q)} = 1$ . This means that the complex exponents lie on the right of the vertical line  $\tau_R(q) = \tau^R(q)$ . In the lattice case,  $\tau(q) = \tau^R(q) + in\omega$  also belong to the set of complex exponents, where  $n \in \mathcal{Z}$  and  $\omega = 2\pi/\ln \lambda$  is the fundamental angular log-frequency of lattice fractals and multifractals. In the non-lattice case,  $\tau(q) = \tau^R(q)$  is the only complex exponent satisfying  $\tau_R(q) = \tau^R(q)$ . Furthermore, there is a right boundary  $\tau_0(q)$  of the set of complex exponents, that is,  $\tau_R(q) < \tau_0(q)$ . (We refer the interested reader to Sec. 2.5 of [42] for a rigorous proof for fractal strings, which can be easily generalized to the present case.) Hence the set of complex exponents lie in a strip  $[\tau^R(q), \tau_0(q)] \times \mathcal{R}$ .

In the case of lattice multifractal, there exists a preferred scaling ratio  $\lambda$  so that equation (37) can be expressed as a polynomial equation (21) with respect to the unknown  $\lambda^{\tau(q)}$  of degree  $\max_j \{k_j\}$ . The set of complex exponents is obtained easily from the set of complex solutions of (21). Hence there are finite complex numbers  $\tau_j(q)$  such that the set of complex exponents is given by

$$\mathcal{T} = \{\tau_j(q) + in\omega, n \in \mathcal{Z}, j = 1, 2, \dots, \ell\}, \quad (39)$$

where  $\ell \leq \max_j \{k_j\}$ . Thus the complex exponents lie on finitely many vertical lines in the complex plane. The points on each vertical line corresponding to a given  $\tau_j(q)$  distributed evenly with spacing  $\omega$ .

Assume that  $(\tau_j)_R \neq (\tau_k)_R$  for  $j \neq k$  and  $\tau_1(q) = \tau^R(q)$ . Then we have

$$(\tau_j)_I = \omega/2, \quad (40)$$

where  $j > 1$ . This result derives because the points on each line are evenly located with spacing  $\omega$  and symmetric with respect to the real axis. The log-frequencies of the moments are thus given by

$$f_{j,n} = \frac{(\tau_j)_I + n\omega}{2\pi} = \begin{cases} n\omega/2\pi, & \text{if } j = 1 \\ (\frac{1}{2} + n)\omega/2\pi, & \text{if } j > 1 \end{cases}, \quad (41)$$

where  $n \in \mathcal{Z} - \{0\}$  when  $j = 1$  and  $n \in \mathcal{Z}$  when  $j > 1$ ,  $f_{1,1}$  is the fundamental log-frequency and  $f_{j>1,0}$  are subharmonics of  $f_{1,1}$  [35]. Certainly, it is also possible that there are at least two complex exponents with indices  $j$  and  $k$  such that  $(\tau_j)_R = (\tau_k)_R$ . In this case, the overall points on line  $\tau_R(q) = (\tau_k)_R$  are no longer evenly spaced with period  $\omega$ . This possibility will be clearer in the following when we approximate a non-lattice multifractal with a sequence of lattice multifractals. It is clear that  $f_{j>1,0}$  might change for different orders  $q$ . Nevertheless,  $f_{1,1} = \omega/2\pi$  holds for any  $q$ . In other words, the fundamental log-frequency of a lattice multifractal is independent of the order  $q$  [38].

In the case of non-lattice multifractals, the set of complex exponents is not periodic. However, the necessary and sufficient condition for the existence of log-periodicity is the existence of periodicity in the plane of the complex exponents associated with a preferred scaling ratio. In the present case, there is no such preferred scaling ratio and hence no log-periodicity. The complex exponents of a non-lattice multifractal can be approximated by the complex exponents of a sequence of lattice multifractals with larger and larger  $\omega$ . The approximation sequence of lattice multifractals can be constructed explicitly, as in the case of fractal strings [42]. This construction process is described in the following Sec. II D 2.

### 2. Approximating non-lattice multifractal by a sequence of lattice multifractals

Let us denote the scaling ratios  $\Lambda$  of the non-lattice multifractal as  $\lambda_j$  where  $j = 1, \dots, n$ . Given any real number  $\lambda_0 > 1$ , we have a set of numbers  $\Theta = \{\theta_j = \ln \lambda_j / \ln \lambda_0 : j = 1, \dots, n\}$ , defining the coordinates of a point in the  $n$  dimensional space  $\mathcal{R}^n$ . Since the multifractal is non-lattice, there is at least one  $j$  such that  $\theta_j$  is an irrational number for any possible choice of  $\lambda_0$ . It is known that there exists a sequence of points  $\Theta^{(k)} = \{\theta_j^{(k)} : j = 1, \dots, n\} \in \mathcal{R}^n$  which converge to  $\Theta$ , where  $\theta_j^{(k)}$  are rational numbers. Obviously, the sequence of rational numbers  $\theta_j^{(k)}$  converge to  $\theta_j$  for every

$j = 1, \dots, n$ . If some  $\theta_j$  is rational, we stipulate trivially that  $\theta_j^{(k)} = \theta_j$  for all  $k$ . Posing  $\lambda_j^{(k)} = \lambda_0^{j^{(k)}}$ , we obtain a sequence of lattice multifractals  $\Lambda^{(k)}$  with scaling ratios  $\{\lambda_j^{(k)} : j = 1, \dots, n\}$  converging to the non-lattice multifractal. The set of complex exponents  $\mathcal{T}^{(k)}$  of  $\Lambda^{(k)}$  converges to the set of complex exponents  $\mathcal{T}$  of  $\Lambda$ . In practice, we can take a lattice multifractal  $\Lambda^{(k)}$  with  $k$  large enough as an approximation of the non-lattice multifractal  $\Lambda$ .

Let us write  $\theta_j^{(k)} = s_j^{(k)} / t_j^{(k)}$  where  $s_j^{(k)}$  and  $t_j^{(k)}$  are relatively prime. Let  $t^{(k)}$  be the minimal common divisor of  $\{t_j^{(k)} : j = 1, \dots, n\}$ . Then  $\lambda^{(k)} = \lambda_0^{1/t^{(k)}}$  is the preferred scaling ratio of  $\Lambda^{(k)}$ . We thus recover the polynomial equation (21):

$$\sum_{j=1}^n m_j^q \left[ \lambda_0^{\tau(q)/t^{(k)}} \right]^{s_j^{(k)} t^{(k)} / t_j^{(k)}} = 1, \quad (42)$$

where  $s_j^{(k)} t^{(k)} / t_j^{(k)}$  are integers. We can choose a sequence ensuring that  $\theta_j^{(k)}$  is monotonous with respect to  $k$ . It follows that  $t^{(k)}$  increases with  $k$ . Therefore, the fundamental log-frequencies  $f^{(k)} = 1 / \ln \lambda^{(k)}$  of  $\Lambda^{(k)}$  increase when converging to  $\Lambda$ . In other words, there is no finite limit of  $f^{(k)}$  when  $k$  tends to  $\infty$  and the fundamental log-frequency of a non-lattice multifractal is thus not defined. Practically, when one investigates the Lomb periodogram of the residuals of a  $q$ -order moment of a non-lattice multifractal, the log-frequency corresponding to the highest Lomb peak is indefinite and increases when the sampling of data points of the moment becomes denser (so as to investigate more scales  $r$ ) [38]. On the other hand, the distance of separation between the complex exponents on each vertical line becomes larger and larger. This is not surprising since the degree  $\max_j \{s_j^{(k)} t^{(k)} / t_j^{(k)}\}$  of the polynomial equation (42) increases with  $k$  implying more vertical lines, some of which may overlap.

### III. NUMERICAL SIMULATIONS ON LATTICE MULTIFRACTALS

In this section, we perform computer simulations to explore the properties of lattice multifractal measures because of the absence of analytic results. Especially, the properties of the log-periodic function  $\psi(r)$  are investigated. This task remains difficult for lattice multifractals with more than three partitions in each generation. With the increase of partition number  $n$ , the iteration number and hence the computational time needed in order to obtain detectable log-periodic structure with relatively low noise level increases exponentially. We thus have to confine our study to small  $n$  values. In Sec. III A, we study binomial measures with fixed amplification factors  $\lambda_1 = (\sqrt{5} + 1)/2$  and  $\lambda_2 = (\sqrt{5} + 3)/2$  and varying measure multipliers  $m_1 = m$  and  $m_2 = 1 - m$  to demonstrate

three scaling regimes: the fractal regime, the crossover regime and the Euclidean regime, the latter resulting from finite size effects. Note that the geometric support is not fractal. Then, we study the properties of the Euclidean regime in Sec. III B, allowing us to gain insight into the structure of the noise stemming from the incomplete construction of the multifractal measure and of the partitioning. In Sec. III C, we study the scaling properties of the amplitude of log-periodic oscillations decorating the scaling of moments.

#### A. Finite size effect

We performed 13 iterations to construct a lattice binomial measure with  $m = 0.2$ . Then the moments  $\Gamma(r, q)$  for different orders  $q$  were calculated based on the box-counting method with size  $r$  in logarithm distributed evenly in  $[e^{-9}, e^{-1}]$ . The log-log plot of  $\Gamma(r, q)$  against  $r$  for  $q = 1$  recovers  $\Gamma(r, q = 1) = 1$  with minor fluctuations of order  $10^{-15}$  stemming from the precision of the computation. This is clear from the definition (11) of the moments and the conservation of measure. The log-log plot of  $\Gamma(r, q)$  versus  $r$  for  $q = 0$  is a perfect straight line with slope  $-D_0 = -1$ . If the geometric support is fractal, the slope should be  $-D_f$ . The log-log plot of  $\Gamma(r, q)$  against  $r$  for  $q \in (0, 1) \cup (1, \infty)$  looks like a strip with slope  $\tau(q)$  which is analogous to Fig. 10. We postpone the discussion of this case till Sec. IV.

Fig. 1 shows the dependence of the moments  $\Gamma(r, q)$  with respect to box size  $r$  in a log-log plot for  $q < 0$ . There are three regimes clearly visible in the figure separated by two vertical dashed lines. The log-periodic oscillations decorate the scaling law in regime *I*. It is easy to calculate numerically the corresponding log-frequency  $f_0 \approx 1 / \ln \lambda = 2.0781$  by employing a spectral analysis on the residuals defined as  $\psi - \langle \psi \rangle$  or on the local derivatives defined in Eq. (22). Regime *III* corresponds to perfect straight lines with different slopes. Regime *II* shows the crossover from large box sizes in regime *I* to small ones in regime *III*. We shall clarify in the sequel that *I* is the fractal regime, *III* is the Euclidean regime and *II* is the crossover regime. We shall see that this phenomena is due to the finite size effect.

It is well known that, although the mathematical model for the construction of a fractal or multifractal measure contains an infinite number of steps of the iterative construction process, the notion that they are (statistically) self-similar can only apply between certain cut-offs in practice [1]. In other words, what we are able to deal with in nature, laboratory and computer simulations are in fact *pre-fractals* and *pre-multifractals*. We nevertheless use the term “fractal” and “multifractal” without the prefix “pre”.

Let  $r_c$  denote the crossover scale (close to the inner cutoff) of a multifractal with measure  $\mu_i = \mu(r_i)$  distributed uniformly on a segment  $\mathcal{F}_i$  of scale  $r_i$ , where

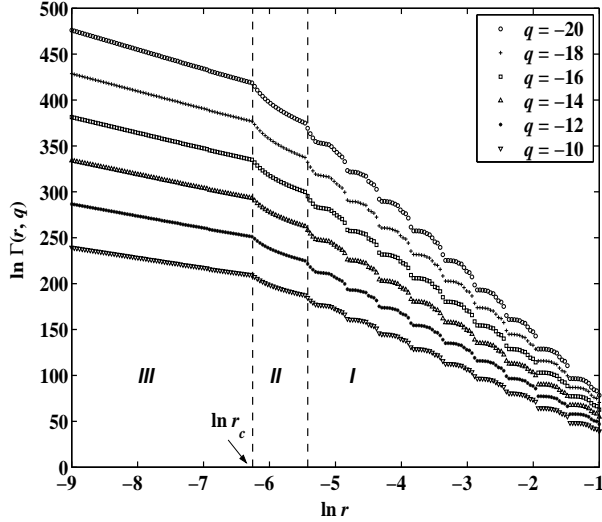


FIG. 1: The dependence of moments  $\Gamma(r, q)$  with respect to box size  $r$  in a log-log plot for  $q < 0$ . The multifractal is a lattice binomial measure with scale multipliers  $\lambda_1 = \sqrt{\lambda_2} = (\sqrt{5} + 1)/2$  and measure multipliers  $m_1 = 1 - m_2 = 0.2$ . We performed 13 iterations to construct the multifractal. There are three regimes clearly visible separated by two vertical dashed lines, where *I* is the fractal regime, *III* is the Euclidean regimes and *II* is the crossover regime. The left vertical line is located precisely at  $r_c = r_1^{1/3}$  (see text for details).

$i = 1, \dots, n$ . It is clear that

$$r_c = (\max\{r_i\})^b, \quad (43)$$

where  $b$  is the iteration number of the construction. This  $r_c$  is the maximal segment among the  $n^b$  segments with uniform measure. Choosing counting boxes with  $r < r_c$ , we have approximately that  $\Gamma(F; r, q) \approx \sum_{i=1}^n \Gamma(\mathcal{F}_i; r, q)$ . There are about  $n_i = r_i/r$  boxes covering segment  $\mathcal{F}_i$ , each box possessing the measure  $\mu_i/n_i$ . Thus, we have  $\Gamma(\mathcal{F}_i; r, q) = n_i(\mu_i/n_i)^q$ . It follows immediately that

$$\Gamma(F; r, q) \approx \sum_{i=1}^n \mu_i r_i^{1-q} r^{q-1}. \quad (44)$$

where  $\sum_{i=1}^n \mu_i r_i^{1-q}$  is independent of the box size  $r$ . We obtain that  $\tau(q) = q - 1$  from the definition (17) and  $D_q = 1$ . Concerning the general situation in a  $d$  dimensional space, we have  $\tau(q) = (q - 1)d$  and  $D_q = d$  in regime *III*, which is completely different from the mono-fractal case obtained from a multifractal which is such that  $D_q = D_0 = D_f$ . We thus find that a pre-fractal is Euclidean if we investigate it at a very high resolution.

We have observed in Fig. 1 that  $r_c$  is precisely the right boundary of the Euclidean regime *III*. The inner cutoff is obviously larger than  $r_c$ , since a box with size greater than  $r_c$  doesn't guarantee the absence of a possible destruction of the log-periodic structure close to  $r_c$ . Indeed, such a box will inevitably split a segment into two parts which introduces errors. However, the inner cutoff can not be determined rigorously but only numerically.

When changing the value of  $m$ , we can still observe four different kinds of moments  $\Gamma(r, q)$  associated with different  $q$ 's: (1)  $q < 0$ , (2)  $q = 0$ , (3)  $q = 1$  and (4)  $q \in (0, 1) \cup (1, \infty)$ . It is apparent that the plots of the moments as a function of  $r$  for (2) and (3) are similar for all lattice and non-lattice multinomial measures, and thus trivial. For the present binomial measure, when  $m$  is large (close to 1), case (1) exhibits a strip while (2) shows three regimes. The discussion for small  $m$  about the three regimes above apply to large  $m$ . When  $m = (\sqrt{5} - 1)/2$ , the measure degenerates to a mono-fractal, where the measure is uniformly distributed over the support with density 1.

## B. Residuals of the moments in the Euclidean regime *III*

Although regime *III* is trivial in the sense that  $\tau(q) = (q - 1)d$ , there are still fine structures stemming from those boxes covering two segments and the rightmost box as well. Let us define residuals in regime *III* as

$$\phi(r, q) = \ln \Gamma(r, q) - (q - 1) \ln r. \quad (45)$$

For different  $q < 0$ , the residuals  $\phi(r, q)$  have similar shapes. Figure 2 plots the residual for  $q = -20$  with respect to  $r$ . We performed  $b = 5$  iterations to construct the binomial measure. We see accelerating oscillations with decaying amplitudes towards  $r = 0$ . The maximal box size is  $r_c = 0.0902$ . We labelled this point as 0. The consecutive points of local minima and local maxima are labelled as  $1, 2, \dots$  in turn as shown in Fig. 2. The coordinates of these points are denoted accordingly  $(r_i, \phi(r_i, q))$  with  $i = 0, 1, 2, \dots$ . The  $n$ -th oscillation is from point  $2n - 2$  through point  $2n - 1$  to point  $2n$ . One can see that the oscillations are similar to each other. We find that

$$\phi(r_{2n}, q) \approx \phi(r_c, q). \quad (46)$$

Note that  $r_0 = r_c$ . The function  $\phi(r_c, q)$  is found to be linear with respect to  $q$  with negative slope.

Figure 3 draws the box sizes  $r_{2n-1}$  and  $r_{2n}$  versus  $n + 1$  in a log-log plot. We find the following power laws:

$$r_{2n-1} = 2r_1(n + 1)^{-1} \quad (47)$$

for  $n \in \mathbb{Z}^+$  and

$$r_{2n} = r_c(n + 1)^{-1} \quad (48)$$

for  $n \in \overline{\mathbb{Z}^-}$ . It is important to note that  $r_{2n-1}$  and  $r_{2n}$  are independent of  $q$  for given binomial measures. For different iterations  $b$ ,  $r_c$  and  $r_1$  are not constant any more. We can determine  $r_{2n}$  analytically by combining Eqs. (43) and (48), while  $r_1$  should be calculated numerically for different  $b$ . Let  $(\delta r)_n = r_{2n} - r_{2n-2}$ , then  $(\delta r)_n = 1/n(n + 1)$ . When  $n \rightarrow \infty$ , it follows that  $(\delta r)_{n+1}/(\delta r)_n \rightarrow 1$ , which means that the oscillations

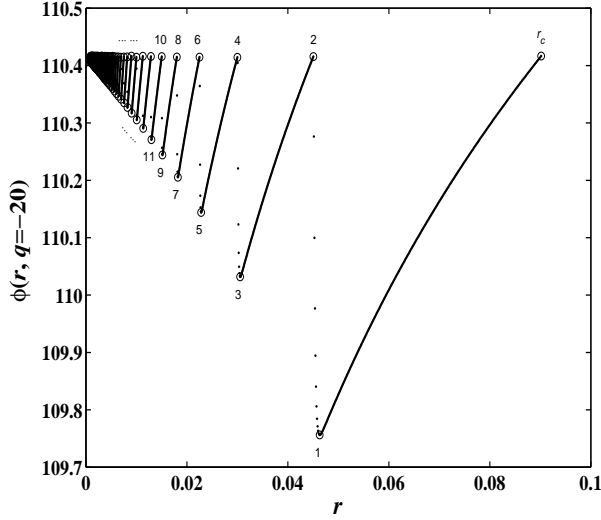


FIG. 2: The dependence of the residual  $\phi(r, q = -20)$  with respect to  $r$ . The even numbers are used to label the points of local maxima, while the odd numbers denote points of local minima. The point 0 is precisely at  $r = r_c$ . It is visible that  $\phi(r_{2n}, q)$  is constant for a given  $q$ .

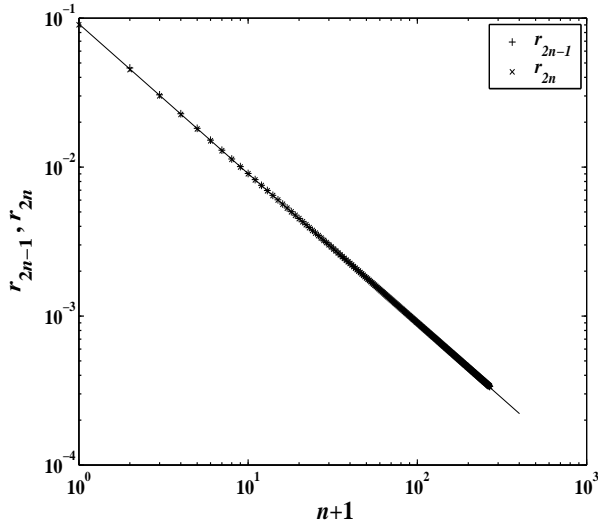


FIG. 3: The power law relationship of  $r_{2n}$  (with  $n \in \mathbb{Z}^-$ ) and  $r_{2n-1}$  (with  $n \in \mathbb{Z}^+$ ) with respect to  $n+1$ . The scaling exponents are  $-1$ .

are approximately periodic locally for large  $n$ . This is not surprised since  $(\delta r)_n$  decays more and more slowly when  $r \rightarrow 0$  following a  $1/n^2$  law.

Define the amplitude of the  $n$ -th oscillation as the distance of point  $(r_{2n-1}, \phi(r_{2n-1}, q))$  to the line  $\phi(r, q) = \langle \phi(r_{2n}, q) \rangle_n$ :

$$h_n(q) = \phi(r_{2n-1}, q) - \langle \phi(r_{2n}, q) \rangle_n, \quad (49)$$

where  $\langle \rangle_n$  is an average over different oscillations  $n$ . Figure 4 shows the dependence of the amplitude  $h_n(q)$  for  $q = -20$  with respect to  $r_{2n}$ . Again, we observe a re-

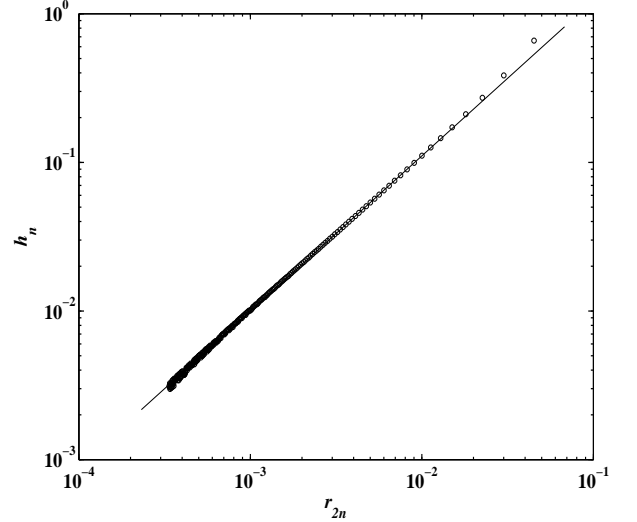


FIG. 4: The power law dependence of the amplitude  $h_n(q)$  with  $q = -20$  versus  $r_{2n}$ . The scaling exponent is  $\alpha = 1.0569$ .

markable power law relationship:

$$h_n(q) = c(q) \cdot r_{2n}^\alpha, \quad \alpha = 1.0569, \quad (50)$$

where

$$c(q) = h_1(q)(r_c/2)^{-\alpha} \quad (51)$$

is a function of  $q$ .

We also investigated the dependence of  $h_1(q)$  with respect to  $q$ , as shown in Fig. 5. It seems that  $h_1(q)$  approaches a constant when  $q$  tends to  $-\infty$ . The points (o) in Fig. 5 can be represented by the following law:

$$h_1(q) = h_1(-\infty) - C/|q|^\beta, \quad (52)$$

where the values  $h_1(-\infty) = 0.6915$ ,  $\beta = 1.0013$ , and  $C = 0.6293$  are obtained from a nonlinear regression procedure. The inset verifies the power law dependence of  $h_1(-\infty) - h_1(q)$  as a function of  $-q$ . We also find that  $h_1(-\infty) = 0.6915$  is universal for different  $b$  and  $m$ , while  $\beta$  and  $C$  vary for different  $b$  and  $m$ . In addition, the amplitude  $h_1(q)$  increases with  $|q|$ .

### C. Residuals of the moments in the fractal regime I

We now study the log-periodic function  $\psi(r, q)$  and the corresponding residuals  $\ln \psi(r, q) = \ln \Gamma(r, q) - \tau(q) \ln r$  of moments in regime I defined in Eq. (19). Denoting  $\lambda_1 = \lambda$ , we find  $\lambda_2 = \lambda^2$ . From (37), we have  $m^q \lambda^{\tau(q)} + (1 - m)^q \lambda^{2\tau(q)} = 1$  which is a solvable univariate second-order equation with respect to  $\lambda^{\tau(q)}$ . The explicit expression of the exponent  $\tau(q)$  follows:

$$\tau(q) = \frac{\ln 2 - \ln \left[ m^q + \sqrt{m^{2q} + 4(1 - m)^q} \right]}{\ln \lambda}, \quad (53)$$



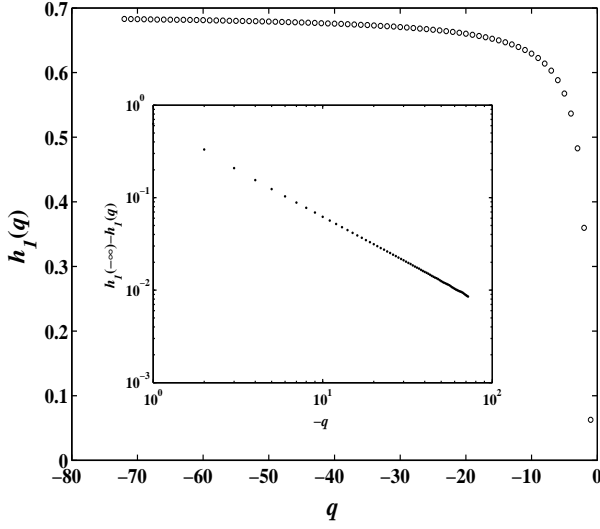


FIG. 5: The dependence of  $h_1(q)$  with respect to  $q$ . There is a limit for  $h_1(q)$  when  $q$  tends to  $-\infty$ . The inset shows the power law dependence of  $h_1(-\infty) - h_1(q)$  versus  $-q$ . The scaling exponent is  $\beta = 1.0013$ .

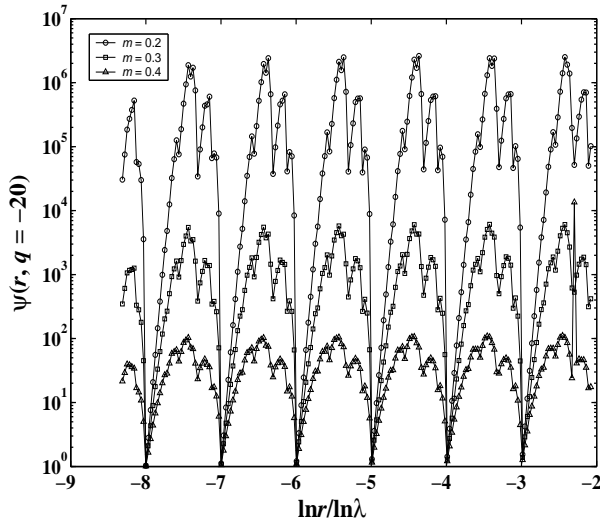


FIG. 6: The dependence of  $\psi(r, q)$  for  $q = -20$  with respect to  $\ln r / \ln \lambda$  for different  $m$ . The periodicity is clearly visible with period  $\ln \lambda$  in  $\ln r$  axis. The amplitude of the oscillations decreases with increasing  $m$  for fixed  $q$ . The local minima are located precisely at  $r = \lambda^{-i}$  with  $i \in \mathbb{Z}^-$ .

where  $\lambda = (\sqrt{5} + 1)/2$  is the preferred scaling ratio. The behavior of  $\psi$  is simpler, since it is strictly periodic in  $\ln r$ . Thus, given  $m$  and  $q$ , the log-periodic oscillations have constant amplitude along  $r$ . Figure 6 shows the dependence of  $\psi(r, q)$  for  $q = -20$  with respect to  $\ln r / \ln \lambda$  for different  $m$ .

The three lines in Fig. 6 are periodic in  $\ln r / \ln \lambda$  with period 1. The amplitudes of the oscillations decrease with increasing  $m$  for fixed  $q$ . The local minima are located precisely at  $r = \lambda^{-i}$  with  $i \in \mathbb{Z}^-$ . The abscissa of the

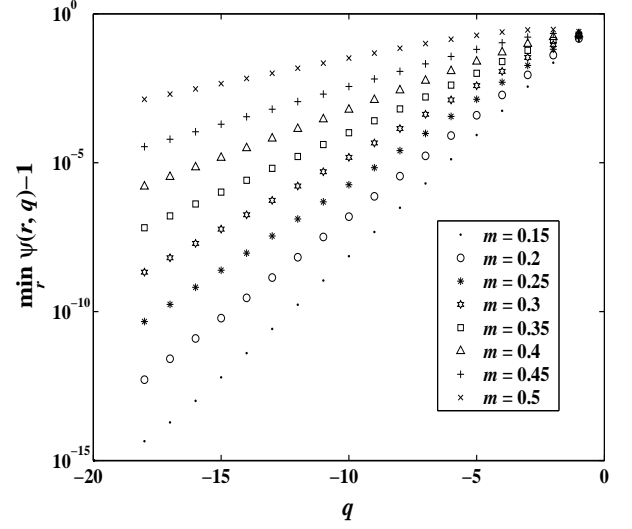


FIG. 7: The exponential approach of  $\min_r \psi(r, q)$  to 1 when  $|q|$  increases for different  $m$  is shown. The slopes of the straight lines are approximately evenly spaced for small  $m$ .

local maxima are different for different  $m$ , while those for same  $m$  but different  $q$  overlap. For large  $r$ , the noise increases with  $m$ . For small  $r$ , the oscillations are gradually spoiled to the right of the crossover regime II, which were not shown in Fig. 6. Hence, it is better to investigate the oscillations in the middle of the fractal regime I to obtain a quantitative description of the log-periodic oscillations of  $\psi(r, q)$ .

As shown in Fig. 6, the local minima  $\min_r \psi(r, q)$  are close to 1 at  $r = \lambda^{-i}$  with  $i \in \mathbb{Z}^-$ . Actually, in the trivial case  $r = 1$ , the moments  $\Gamma(r, q)$  are always equal to 1 for all kinds of conservative multifractal measures and all orders  $q$ . We calculated the values of  $\min_r \psi(r, q)$  for different  $q$  and  $m$ . The results are shown in Fig. 7. We find that  $\min_r \psi(r, q)$  approaches closer and closer to 1 with the increase of  $|q|$  or the decrease of  $m$ . The distance of the minima  $\min_r \psi(r, q)$  to 1 is exponential as a function of  $q$  for fixed  $m$ . The slopes of the straight lines fitted to the data for each  $m$  in Fig. 7 are approximately evenly spaced for small  $m$ . This verifies the analytic results that  $\psi(\lambda^{-i}) = 1$ .

Figure 8 shows the local maxima  $\max_r \psi(r, q)$  versus  $q$  for different  $m$ . Note that moments of larger  $m$  contain a large noise amplitude making the numerical determination of local maxima rather difficult. We find that  $\max_r \psi(r, q)$  increases exponentially with  $|q|$ . This result still holds for other lattice multifractal measures. The slopes of the straight lines fitted to the data for each  $m$  in the log-linear plot of Fig. 8 are proportional to  $\ln m$ .

We define the amplitude of log-periodic oscillations as

$$h(q) = \max_r \psi(r, q) - \min_r \psi(r, q). \quad (54)$$

It is easy to see that  $h(q)$  has a behavior similar to that of  $\max_r \psi(r, q)$ . It follows the important result that the

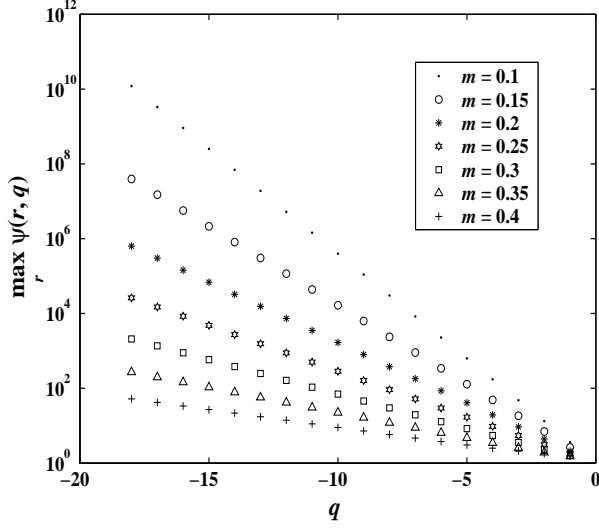


FIG. 8: The exponential dependence of  $\max_r \psi(r, q)$  as a function of  $q$  for different  $m$ . The slopes of the straight lines in this log-linear plot are proportional to  $\ln m$ .

amplitude of the log-periodic oscillations of lattice multinomial measures increases with  $|q|$ . A similar result is known for (lattice) fractals [28].

#### IV. A NOVEL APPROACH FOR EXTRACTING LOG-FREQUENCY

A natural question arises in practice concerning the determination of the log-frequency and thus the preferred scaling ratio in the detection of log-periodicity in fractals or multifractals. Up to now, five different methods have attempted to improve the detection of log-periodicity [38]. The common part of four non-parametric methods is the Lomb periodogram analysis. The Lomb analysis of  $\psi(r, q)$  in Fig. 6 gives a very significant peak at log-frequency  $f_0 = 1/\ln \lambda$ . Here, we study more complicated measures for which the log-periodic oscillations are not visible to the bare eyes but can still be detected by spectral analysis. We develop in this section a novel method for the detection of log-frequencies, which is expected to be powerful also more generally in the search of log-periodicity in real systems.

We construct a triadic multifractal measure which has three partitions in each generation with scaling ratios  $\lambda_1 = 2$  and  $\lambda_2 = \lambda_3 = 4$  and measure multipliers  $m_1 = m_3 = 0.5$  and  $m_2 = 0$ . The measure is carried by the generalized Cantor set. Thus the preferred scaling ratio is  $\lambda = 2$  and the fundamental log-periodic frequency is  $f_0 = 1/\ln 2$ . The analytic value of  $\tau(q)$  is also given by (53) with  $m = 0.5$  and  $\lambda = 2$ . We performed  $n = 11$  iterations for the construction of the measure. Again, the counting box size is evenly sampled in the logarithm of the scale. The moments  $\Gamma(r, q)$  of the measure were thus calculated for different orders  $q$  based on the box-

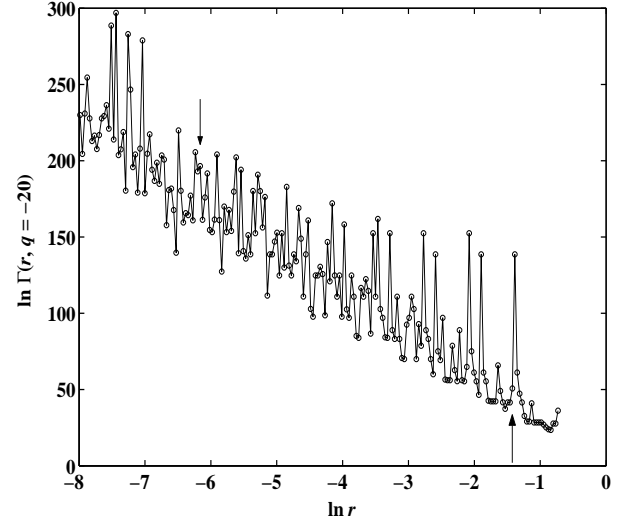


FIG. 9: The dependence of  $\ln \Gamma(r, q)$  with respect to  $\ln r$  for  $q = -20$ . Although the plot is very noisy, a linear least square fitting gives a slope close to the analytic exponent  $\tau(q)$ . No unambiguous (log-)periodic oscillations are visible.

counting method.

We present in Fig. 9 a typical plot of  $\ln \Gamma(r, q)$  versus  $\ln r$  for  $q < 0$ . Although the plot is very noisy, a linear least square fitting gives a slope close to the analytic exponent  $\tau(q)$ . No unambiguous simple (log-)periodic oscillations are visible. Since  $\ln r_c = -n \ln \lambda_1 = -7.62$ , we restricted the interval of study to  $-6.17 < \ln r$ , where the lower bound is indicated by the left downward arrow in Fig. 9. Indeed, a behavior different from large  $r$  can be observed for small  $r$ . We also introduced an outer cutoff in the large  $r$  range as indicated by the right upward arrow in Fig. 9. Our analysis of log-periodicity detection was thus carried out in the interval confined within the two arrows, containing a total of  $N = 131$  data points. Note that a different but reasonable choice of this interval doesn't impact on the results.

Fig. 10 shows a typical plot of  $\ln \Gamma(r, q)$  versus  $\ln r$  for  $q > 1$ . A linear least square fit of the points recovers a numerical estimate of  $\tau(q)$  which is close to the theoretical value. The plot also exhibits many parallel patterns (rectangle-like) which are arranged periodically in  $\ln r$ , as indicated by the arrows. We find that the period is approximately  $2 \ln \lambda$ , which is interpreted as the frequency of a subharmonic to the fundamental log-frequency. A similar subharmonic log-periodic frequency was also reportedly detected in the growing diffusion-limited aggregation clusters [35]. However, the Lomb periodogram of the detrended  $\ln \Gamma(r, q)$  in Fig. 10 doesn't provide convincing signal of such  $f_0/2$  subharmonic (not shown). We nevertheless observed in the Lomb periodogram two outstanding peaks at log-frequencies  $f = 11.54$  and  $f = 15.87$ , although this observation does not ensure the statistical significance of log-periodicity. Lower order moments provide more significant Lomb periodogram when

$q > 0$ , which means that the noise was amplified rapidly for large  $q$ 's. On the other hand, the impact of  $q$  on the noise is less important when  $q < 0$ . This noise amplification effect of larger  $q$  suggests to investigate lower-order moments to detect log-periodicity.

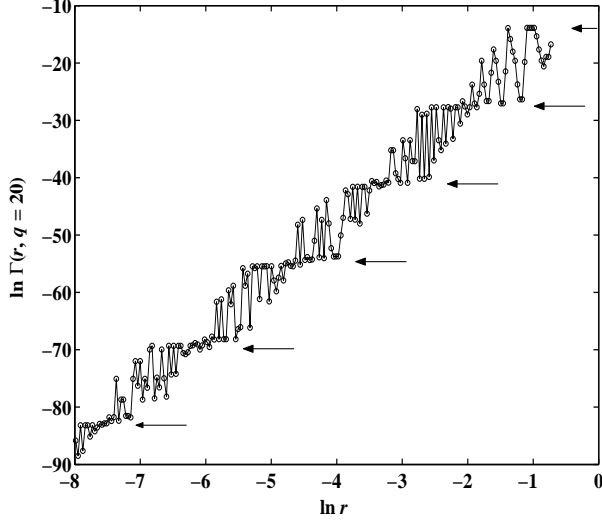


FIG. 10: The dependence of  $\ln \Gamma(r, q)$  with respect to  $\ln r$  for  $q = 20$ . The arrows indicate a periodic pattern in  $\ln r$ . The period is  $2 \ln \lambda$  which is interpreted as a subharmonic of the fundamental log-frequency.

We detrended the moment  $\ln \Gamma(r, q = -3)$  to remove the power-law scaling. Here the scaling exponent is estimated directly from the data points and the resultant residuals have zero mean. This method was used extensively in practice (this method is different from that used in Sec. IIIB and IIIC). Analyzing these residuals by the Lomb method gives a Lomb periodogram shown in Fig. 11. It is interesting to point out that the Lomb periodogram is periodic of period  $19/\ln \lambda = 27.4112$ . The local detail around  $f = 27.4112$  is shown in the right inset of Fig. 11. We see a clear burst exactly at  $f = 27.4112$  causing the discontinuity at this point. It is necessary to stress that this burst itself is not a Lomb peak. It is thus sufficient to analyze only the  $f < 27.4112$  part of the periodogram as shown in Fig. 11. In addition, the Lomb periodogram in Fig. 11 is apparently symmetric with respect to  $f = 9.5/\ln \lambda = 13.7056$ . The left inset shows the local detail around  $f = 13.7056$ , which is a discontinuous burst as well. This is the reason why the right inset is symmetric with respect to  $f = 27.4112$ .

In Fig. 11, the two highest peaks are located at  $f = 11.54$  and  $f = 15.87$ . This is what we can see in the Lomb periodogram for  $q > 1$  as we alluded above. The claim that the fundamental logarithm frequency is  $f_0 = 11.54$  or  $f_0 = 15.87$ , as done in many other practical systems, has a false-alarm probability of 0.006% assuming that the noise is independent and Gaussian [45, 46]. The existence of two peaks of the same height and the symmetric structure of the Lomb periodogram reinforce further

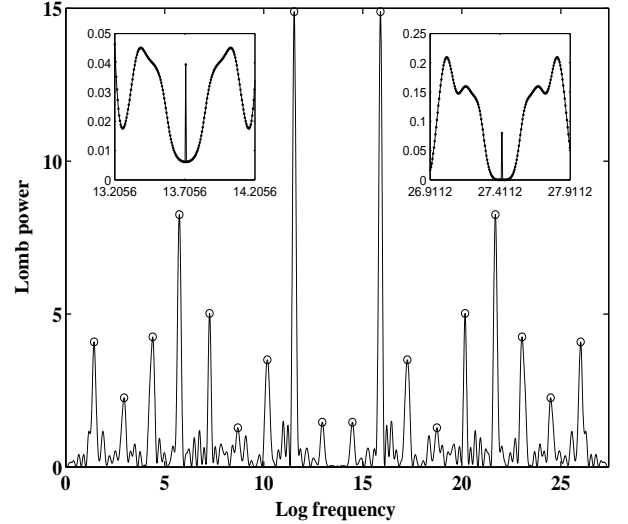


FIG. 11: The Lomb periodogram of the residuals of the  $q = -3$  order moment. The left inset shows the local details around  $f = 9.5/\ln \lambda$ , which is the symmetric axis of the periodogram. The right inset shows the local details around  $f = 19/\ln \lambda$ , beyond which the Lomb periodogram duplicates itself periodically. The Lomb peaks indicated by open circles are approximately evenly spaced.

the statistical significance of the existence of a genuine log-periodicity.

An additional important evidence is offered by expanding  $\psi(r, q)$  in the Fourier space, which identifies a discrete set of log-frequencies  $f_n$  with amplitudes  $A_n$ . Here, we find that the amplitudes  $A_n$  of different frequencies  $f_n$  are not restricted to a presumed inequality that  $A_1 > A_n$  with  $n > 1$  (we refer to [47] for a detailed discussion). In the case where several  $A_n$  are comparable, as shown in Fig. 11, we have to study the harmonics of the fundamental frequency. There are indeed many slim peaks in Fig. 11 that are approximately evenly spaced. We indicated these 18 peaks with open circles, whose corresponding log-frequencies are denoted as  $f_n$ . This recognition process is objective, since all except the 6th and 13th peaks are higher than the remaining peaks. It is quite reasonable to interpret  $f_n$  as the  $n$ -th harmonic of the fundamental log-frequency. A convenient estimate of  $f_0$  is the mean of the differences of consecutive frequencies. This gives  $f_0 = \langle f_n - f_{n-1} \rangle = 1.4457 \pm 0.0671$ . In addition, we can expect that  $f_n \approx n f_0$ . Thus, we can take the slope of the line fitted to points  $(n, f_n)$  as another estimate of  $f_0$ . Figure 12 plots  $f_n$  as a function of  $n$ , which exhibits an almost perfect linear relationship. The slope of the fitted line is  $f_0 = 1.4396 \pm 0.0005$ . The estimates of  $f_0$  from the two approaches are comparable to each other and both in excellent agreement with the theoretic value of  $f_0 = 1.4427$ . However, the linear regression method of Figure 12 is obviously much more stable. The preferred scaling ratio is thus calculated to be  $\lambda = e^{1/f} = 2.0030$  with  $\sigma_\lambda = \sigma_f e^{1/f} / f^2 = 0.0005$ .

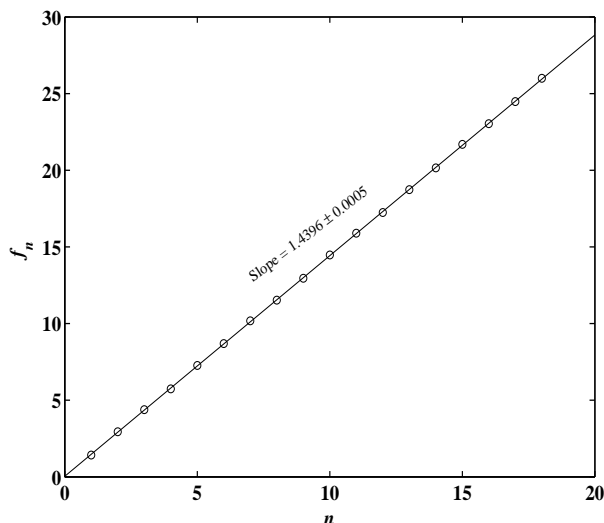


FIG. 12: The linear dependence of log-frequencies  $f_n$  of the harmonics of the fundamental frequency  $f_0$  as a function of their order  $n$ . The slope of the fitted straight line is  $1.4396 \pm 0.0005$  providing an estimate of  $f_0$  in excellent agreement with the theoretic value of  $f_0 = 1/\ln 2$ . The preferred scaling ratio is thus  $\lambda = 2.0030 \pm 0.0005$  having only a 0.3% deviation from the true value of  $\lambda = 2$ .

In real systems, it is possible that the Lomb periodogram is much more noisy than found in Fig. 11. In that case, we may only determine a few but not all harmonics, so that the successively detected harmonics are not consecutive. In this case, taking the differences between successively detected harmonics will not give a constant value equal to the fundamental log-frequency. This certainly increases the difficulty of the detection of log-periodicity and lowers the significance of the extracted log-frequency. One should thus estimate subjectively the possible order of the detected harmonics and reconstruct the best match according to a linear fit such as in Figure 12 but with holes for the missing harmonics. Notwithstanding its difficulties, this method was successfully applied to the search of log-periodic in the energy dissipation of three dimensional fully developed turbulence [38].

## V. CONCLUDING REMARKS

We have derived in this paper the basic discrete scale invariance equations concerning the moments  $\Gamma(r, q)$  of fractals, multifractal measures and joint multifractal measures based on the presence of (statistical) self-similarity in these objects. There exist a set  $\mathcal{T}$  of complex dimensions for fractals and complex exponents for multifractals, corresponding to the set of complex solutions of the corresponding DSI equation. The set  $\mathcal{T}$  lies in a strip  $[\tau^R(q), \tau_0(q)] \times \mathcal{R}$  in the complex plane and is symmetric with respect to the real axis, where  $\tau^R(q) \in \mathcal{T}$  is the only exponent on the real axis.

In the lattice case, the complex exponents are located evenly with spacing  $\omega$  (where  $\omega$  is the fundamental angular log-frequency) on finitely many vertical lines in the complex plane. Corresponding to the complex exponents on the vertical line  $\tau(q) = \tau^R(q)$ , we can obtain a log-periodic expression of  $\Gamma(r, q)$  with a fundamental log-frequency  $f = 1/\ln \lambda$ , where  $\lambda$  is the preferred scaling ratio. We have further verified the log-periodicity in multifractals numerically and proposed a novel precise approach for the extraction of  $f$ . Our simulations also show that the signal-to-noise ratio of the moments increases with  $|q|$  when  $q < 0$  or  $q > 0$ . Since larger signal-to-noise ratio corresponds to more significant Lomb peak, we should investigate lower-order moments to extract log-frequencies, which is independent of the fact that higher-order moments have larger amplitudes of oscillations.

In the non-lattice case, the complex exponents are irregularly located in the strip and  $\tau^R(q)$  is the unique complex exponent in the vertical line  $\tau(q) = \tau^R(q)$ . There are thus no preferred scaling ratio and no exact log-periodicity. However, we can construct a sequence of lattice multifractals whose preferred scaling ratios converge to 1 from above to approximate the non-lattice multifractal so that the set of these lattice multifractals converge to the set of complex exponents of the non-lattice multifractal. We have proposed an explicit algorithm for the construction of the lattice sequence.

Therefore, we can recognize lattice fractals and/or multifractals by the confirmation of log-periodicity in real systems. We can obtain a preferred scaling ratio  $\lambda$  based on spectral analysis. This search not only sheds new light towards a better understanding of the system under study but also offers a constraint on the modelling of the system. Of course,  $\lambda$  does not contain a detailed information on all the scaling ratios  $\lambda_i$ . The search for log-periodicity has been carried out in several real systems, such as in the growing diffusion-limited aggregation (DLA) clusters [35], in two dimensional free decaying turbulence [37] and in three dimensional fully developed turbulence [38, 48]. It is interesting that the preferred scaling ratio is  $\lambda \approx 2$  for the cases of DLA and 3D turbulence and it is possible that the log-frequency  $f_0 = 4 \sim 5$  in the two dimensional free decaying turbulence case [37] turns out to be a harmonic of  $f_0 = 1/\ln 2$ . However, we have to stress that the existence of a preferred scaling ratio  $\lambda$  does not imply that there is only one scaling ratio equal to the measured  $\lambda$ . For instance,  $\lambda = 2$  found in 3D turbulence does not mean that the  $p$ -model [49] is the correct and only one model. We shall further clarify this point by taking the growing DLA clusters as an example as follows.

There are many models proposed to explain the fractal growth of DLA clusters, such as the hierarchical ghost model [50, 51] and the Fibonacci model [52, 53, 54]. In the hierarchical ghost model, pairs of single particles collide and aggregate to form dimers. Then pairs of dimers collide and aggregate to form four-particle clusters. This hierarchical growth process goes on and on to form even-

tually a large DLA cluster. Defining  $b(N)$  as the average number of bonds along the connecting pathway between two particles on an  $N$ -particle cluster, we obtain the DSI equation [50]

$$b(2N) = \frac{3}{2}b(N). \quad (55)$$

Since the average radius  $R$  of a  $N$ -particle cluster obeys  $R \sim \sqrt{b(N)}$  and  $N \sim R^D$ , we have  $D = 2 \ln 2 / \ln(3/2)$  and the set of complex exponents with respect to (55) is

$$\mathcal{T} = \{2/D + 2\pi ni / \ln 2, n \in \mathcal{Z}\}. \quad (56)$$

It is clear that  $\lambda = 2$  and the set of complex exponents is on a vertical line with abscissa of  $2/D$  in the complex plane. On the other hand, by applying the results of the wavelet transform modulus maxima (WTMM) representation to the DLA azimuthal Cantor set, it follows that the number  $N(a)$  of maxima of the WTMM skeleton at scale  $a$  satisfies the Fibonacci rule [52, 53, 54]:

$$N(a) = N(\lambda a) + N(\lambda^2 a). \quad (57)$$

It is easy to show that the set of complex dimensions is [35, 42]

$$\mathcal{D} = \left\{1 + \frac{\ln \phi}{\ln \lambda} + i \frac{2\pi n}{\ln \lambda}\right\} \cup \left\{1 - \frac{\ln \phi}{\ln \lambda} + i \frac{(2n+1)\pi}{\ln \lambda}\right\}, \quad (58)$$

where  $n \in \mathcal{Z}$  and  $\phi = (\sqrt{5} + 1)/2$  is the golden mean. We see that there are two vertical lines in the complex plane in this model. Numerical simulations [35] lead to the identification of two log-frequencies  $f_0 = 1/\ln \lambda$  and  $f_0/2$  in excellent agreement with the prediction of the Fibonacci model. The preferred scaling ratio was estimated numerically to be  $\lambda = 2.2$ . It shows that the Fibonacci model with two scaling ratios  $\lambda$  and  $\lambda^2$  provides a better description than the hierarchical ghost model in the sense of discrete scale invariance.

- 
- [1] B. B. Mandelbrot, *The Fractal Geometry of Nature* (W. H. Freeman and Company, New York, 1983).
  - [2] B. B. Mandelbrot, *J. Fluid Mech.* **62**, 331 (1974).
  - [3] P. Grassberger, *Phys. Lett. A* **97**, 227 (1983).
  - [4] H. G. E. Hentschel and I. Procaccia, *Physica D* **8**, 435 (1983).
  - [5] U. Frisch and G. Parisi, in *Turbulence and Predictability in Geophysical Fluid Dynamics*, edited by M. Gil, R. Benzi, and G. Parisi (North-Holland, 1985), pp. 84–88.
  - [6] T. C. Halsey, M. H. Jensen, L. P. Kadanoff, I. Procaccia, and B. I. Shraiman, *Phys. Rev. A* **33**, 1141 (1986).
  - [7] J. Lee and H. E. Stanley, *Phys. Rev. Lett.* **61**, 2945 (1988).
  - [8] R. Blumenfeld and A. Aharony, *Phys. Rev. Lett.* **62**, 2977 (1989).
  - [9] S. Schwarzer, J. Lee, A. Bunde, S. Halvin, H. E. Roman, and H. E. Stanley, *Phys. Rev. Lett.* **65**, 603 (1990).
  - [10] B. B. Mandelbrot, *Physica A* **168**, 95 (1990).
  - [11] B. B. Mandelbrot, C. J. G. Evertsz, and Y. Hayakawa, *Phys. Rev. A* **42**, 4528 (1990).
  - [12] R. H. Riedi, *J. Math. Analysis Appl.* **189**, 462 (1995).
  - [13] R. H. Riedi and B. B. Mandelbrot, *Adv. Appl. Math.* **16**, 132 (1995).
  - [14] K. J. Falconer and T. C. O’Neil, *Proc. Royal Soc. London A* **452**, 1433 (1996).
  - [15] W.-X. Zhou and Z.-H. Yu, *Physica A* **294**, 273 (2001).
  - [16] W.-X. Zhou, H.-F. Liu, and Z.-H. Yu, *Fractals* **9**, 317 (2001).
  - [17] T. Huillet and A. Porzio, *Fractals* **9**, 129 (2001).
  - [18] W.-X. Zhou and Z.-H. Yu, *Phys. Rev. E* **63**, 016302 (2001).
  - [19] B. B. Mandelbrot, *Pure Appl. Geophys.* **131**, 5 (1989).
  - [20] B. B. Mandelbrot, *Physica A* **163**, 306 (1990).
  - [21] B. B. Mandelbrot, *Proc. Royal Soc. London A* **434**, 79 (1991).
  - [22] M. E. Cates and T. A. Witten, *Phys. Rev. A* **35**, 1809 (1987).
  - [23] A. B. Chhabra and K. R. Sreenivasan, *Phys. Rev. A* **43**, 1114 (1991).
  - [24] A. B. Chhabra and K. R. Sreenivasan, *Phys. Rev. Lett.* **68**, 2762 (1992).
  - [25] W.-X. Zhou and Z.-H. Yu, in *Emergent Nature: Patterns, Growth and Scaling in the Sciences*, edited by M. M. Novak (World Scientific, Singapore, 2002), pp. 434–435.
  - [26] L. Olsen, *Hiroshima Math. J.* **29**, 435 (1999).
  - [27] L. Olsen, *Prog. Probab.* **46**, 3 (2000).
  - [28] L. A. Smith, J. D. Fournier, and E. A. Spiegel, *Phys. Lett. A* **114**, 465 (1986).
  - [29] D. Sornette, *Phys. Rep.* **297**, 239 (1998).
  - [30] A. Johansen and D. Sornette, *Int. J. Mod. Phys. C* **9**, 433 (1998).
  - [31] A. Johansen and D. Sornette, *European Phys. J. B* **18**, 163 (2000).
  - [32] W.-X. Zhou and D. Sornette, *Phys. Rev. E* **66**, 046111 (2002).
  - [33] A. Johansen, H. Saleur, and D. Sornette, *European Phys. J. B* **15**, 551 (2000).
  - [34] Y. Huang, H. Saleur, and D. Sornette, *J. Geophys. Res.* **B 105**, 28111 (2000).
  - [35] D. Sornette, A. Johansen, A. Arneodo, J.-F. Muzy, and H. Saleur, *Phys. Rev. Lett.* **76**, 251 (1996).
  - [36] E. A. Novikov, *Phys. Fluids A* **2**, 814 (1990).
  - [37] A. Johansen, D. Sornette, and A. E. Hansen, *Physica D* **138**, 302 (2000).
  - [38] W.-X. Zhou and D. Sornette, *Physica D* **165**, 94 (2002).
  - [39] D. Sornette, *Why Stock Markets Crash: Critical Events in Complex Financial Systems* (Princeton University Press, Princeton, 2002).
  - [40] R. Badii and A. Politi, *Phys. Lett. A* **104**, 303 (1984).

- [41] G. M. Zaslavsky, *Physica A* **288**, 431 (2000).
- [42] M. Lapidus and M. van Frankenhuysen, *Fractal Geometry and Number Theory: Complex Dimensions of Fractal Strings and Zeros of Zeta Functions* (Birkhäuser, Boston, 2000).
- [43] P. Grassberger and I. Procaccia, *Physica D* **9**, 189 (1983).
- [44] K. J. Falconer, *J. Theor. Probab.* **7**, 681 (1994).
- [45] J. H. Horne and S. L. Baliunas, *Astrophys. J.* **302**, 757 (1986).
- [46] W. Press, S. Teukolsky, W. Vetterling, and B. Flannery, *Numerical Recipes in FORTRAN: The Art of Scientific Computing* (Cambridge University Press, Cambridge, 1996).
- [47] W.-X. Zhou and D. Sornette, *Int. J. Mod. Phys. C* **13**, 137 (2002).
- [48] D. Sornette, in *Proceedings of the Seventh European Turbulence Conference*, edited by U. Frisch (Kluwer, 1998).
- [49] C. Meneveau and K. R. Sreenivasan, *Phys. Rev. Lett.* **59**, 1424 (1987).
- [50] R. C. Ball and T. A. Witten, *J. Stat. Phys.* **36**, 873 (1984).
- [51] T. A. Witten and M. E. Cates, *Science* **232**, 1607 (1986).
- [52] A. Arneodo, F. Argoul, E. Bracy, and J.-F. Muzy, *Phys. Rev. Lett.* **68**, 3456 (1992).
- [53] A. Arneodo, F. Argoul, J.-F. Muzy, and M. Tabard, *Phys. Lett. A* **171**, 31 (1992).
- [54] A. Arneodo, F. Argoul, J.-F. Muzy, M. Tabard, and E. Bracy, *Fractals* **1**, 629 (1993).